Sequence of Quantum Phase Transitions in $Bi_2Sr_2CaCu_2O_{8+\delta}$ Cuprates Revealed by *In Situ* Electrical Doping of One and the Same Sample

Th. Jacobs,[1] Y. Simsek,[1,2] Y. Koval,[2] P. Müller,[2] and V. M. Krasnov[1,*]
[1]Department of Physics, Stockholm University, AlbaNova University Center, SE-10691 Stockholm, Sweden
[2]Department of Physics, Universität Erlangen-Nürnberg, D-91058 Erlangen, Germany
(Received 23 October 2015; published 9 February 2016)

Our recently discovered electrical doping technique allows a broad-range variation of carrier concentration without changing the chemical composition. We show that it is possible to induce superconductivity in a nondoped insulating sample and to tune it reversibly all the way to an overdoped metallic state. This way, we can investigate the whole doping diagram of one and the same sample. Our study reveals two distinct critical points. The one at the overdoped side is associated with the onset of the pseudogap and with the metal-to-insulator transition in the c-axis transport. The other at optimal doping is associated with the appearance of a “dressed” electron energy. Our study confirms the existence of multiple phase transitions under the superconducting dome in cuprates.

DOI: 10.1103/PhysRevLett.116.067001

High-temperature superconductivity in cuprates appears upon the doping of a parent Mott insulator. With increasing doping, cuprates evolve from insulators to poorly metallic materials with a persisting pseudogap (PG) [1–8] in an underdoped state, to strange metals with non-Fermi liquid behavior at optimal doping, and finally to conventional metals with a low T_c in an overdoped state. Understanding the corresponding evolution of the electronic system is important to understanding not only unconventional superconductors but also a broad range of other strongly correlated materials.

Of particular interest is the underdoped state characterized by a coexistence of various competing orders. Such competition often leads to quantum phase transitions, which are considered to be essential for unconventional superconductivity [9,10]. However, the position and the possible nature of such transitions, as well as their role for superconductivity in cuprates, are still under debate. To a large extent this is connected to problems in the interpretation of the pseudogap, which can be connected with various phenomena: short-range antiferromagnetism [3], orbital magnetism [11], stripes [12], charge or spin density waves [13], quadrupole-density waves [10], pair density waves [14,15], crystal lattice reconstruction [16], Fermi surface reconstruction [17], and a precursor superconductivity state [18,19]. Investigation of the doping diagram should allow for the distinction of different pseudogap scenarios [2] (for further discussion, see the Supplemental Material [20]). Unfortunately, different doping diagrams have been deduced from different experiments. This may indicate either that there are multiple coexisting phenomena or that there are technique-specific artifacts and sample-to-sample variations. Therefore, one would ideally like to investigate the whole doping diagram using the same sample and technique.

In this Letter we study the doping diagram of $Bi_2Sr_2CaCu_2O_{8+\delta}$ (Bi-2212) cuprates using intrinsic tunneling spectroscopy [8,48–50]. We employ our recently discovered electrical doping by current injection (I doping) [51–53] for *in situ* changing of the carrier concentration. This allows reversible tuning of the doping state between nondoped insulating and overdoped metallic states. This way, we analyze the doping diagram using one and the same sample. The high precision of doping allows us to suggest two distinct critical points at rather different energy scales.

We study two types of microstructures made of Bi-2212 single crystals. Sample fabrication and experimental details can be found elsewhere [6,20,51,53]. The two types of samples have their advantages and disadvantages. Zigzag structures [see Fig. 1(a)] allow accurate measurements of c-axis characteristics, without spurious contributions from the contacts, but they are prone to self-heating. Small mesas [see Fig. 1(b)] have good thermal anchoring but inevitably include a deteriorated surface layer. Comparison of the two types of structures allows for the exclusion of possible artifacts. We present data for three batches of crystals. Zigzag and mesa structures are made from two different batches with optimal T_c of $\simeq 91$ and $\simeq 82$ K, respectively. We also make a comparison with oxygen (O)-doped $Bi_2Sr_2Ca_{1-x}Y_xCu_2O_{8+\delta}$ crystals [Bi(Y)-2212] with an optimal $T_c \simeq 95$ K.

Application of a large bias ~2–3 V to a microstructure leads to a gradual change of the doping state [51,52]. The corresponding electric field $E \gtrsim 10^8$ V/m is comparable—or even exceeds—values achievable during electrostatic doping with ferroelectric [54] or ion-liquid [55–57] gates. The phenomenon may be due to the electrostatic charging of insulating BiO layers, resulting in a floating gate effect [51], or to charge transfer at a characteristic energy ~1 eV

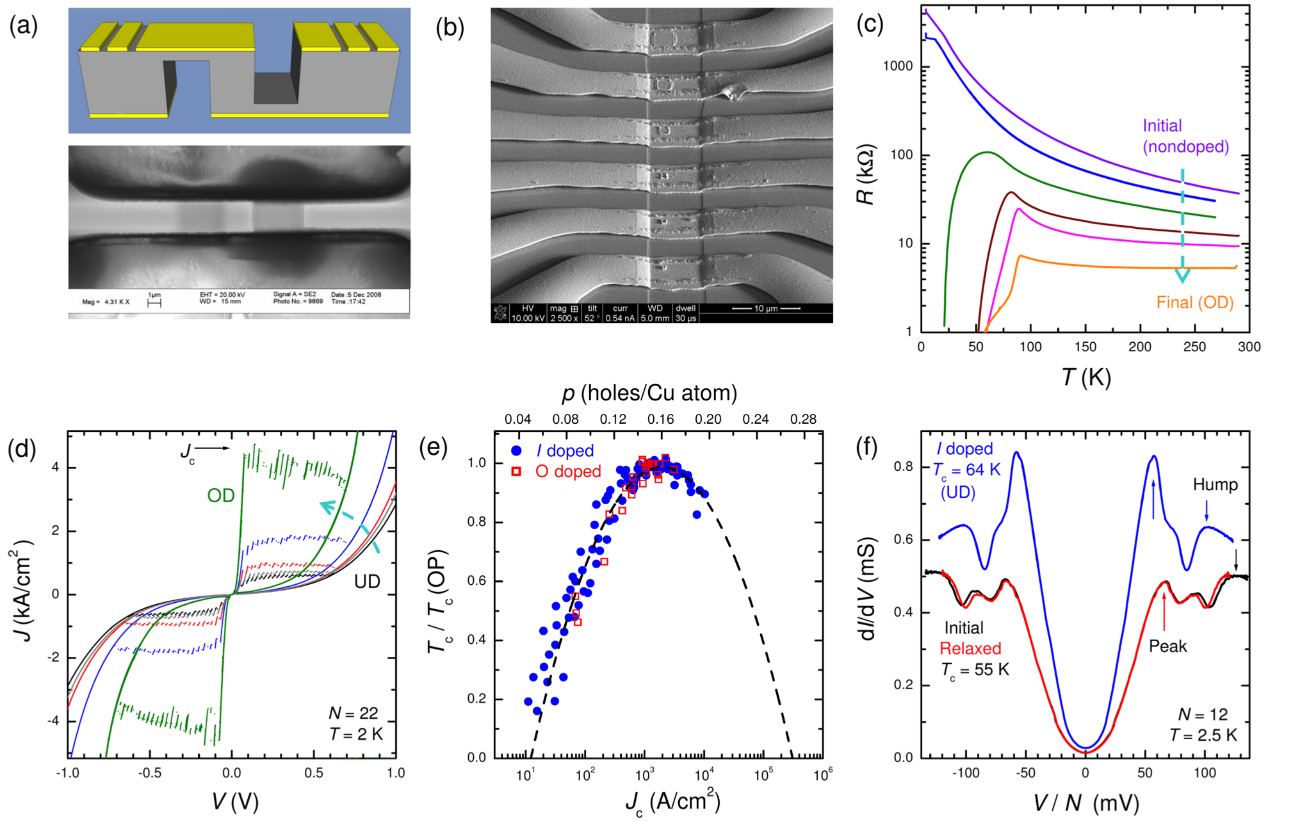

FIG. 1. Sketch and SEM images of (a) a zigzag structure and (b) a crystal with six mesa structures on top. (c) Resistive transition $R(T)$. (d) Current density vs voltage for mesa 1 at different doping states from the initial underdoped to the final overdoped state. Note the strong increase of the Josephson critical current density J_c. (e) T_c vs the logarithm of J_c (the bottom axis) for I-doped zigzag structures and O-doped mesas. The dashed line represents T_c vs doping (the top axis). (f) dI/dV characteristics of mesa 2 at an initial strongly underdoped state (the black line), after I doping (the blue line), and after relaxation at $T \simeq 300$ K (the red line).

[52], as in the case of photodoping [58,59]. The doping state can be increased or decreased reversibly by changing the bias conditions [51–53]. Unlike the ordinary field effect, I doping changes not only the surface layer but also the whole volume of the microstructure. Since the sample is remaining in a cryostat without exposure to oxygen, I doping is not associated with changes of the chemical composition.

Figure 1(c) shows the temperature dependence of zero-bias resistance $R(T)$ for a zigzag structure after sequential I-doping steps. The initial state is insulating. Doping leads to a decrease of resistance and to the appearance of superconductivity. With further doping, T_c is increasing up to a maximum and then starts to decrease, indicating that the structure becomes overdoped. Upon doping, the resistance decreases by several decades and changes the T dependence from semiconductor type to metallic, consistent with its behavior upon oxygen doping [49,60].

Figure 1(d) shows low-bias sections of current density versus voltage ($J-V$) characteristics of mesa 1 after subsequent I-doping steps. It starts with an underdoped state ($p \simeq 0.12$, the black curve) and ends with an overdoped state ($p \simeq 0.176$, the olive curve). The mesa contains $N = 22$ intrinsic junctions. Branches due to one-by-one switching of junctions from the superconducting to the resistive state are clearly seen. The branches remain periodic, indicating a good uniformity of doping within the mesa. From Fig. 1(d) it can be seen that the Josephson critical current density J_c rapidly increases with doping [8,48–50]. In Fig. 1(e) we plot T_c as a function of J_c in a logarithmic scale. The solid blue symbols represent the data for I-doped zigzag structures, while the open red symbols represent the O-doped mesas in Ref. [8]. It can be seen that T_c vs $\ln(J_c)$ has an inverted parabolic dependence, typical for T_c vs p, as shown by the dashed line; i.e., J_c increases exponentially with doping. In what follows we use the strong $J_c(p)$ dependence for an accurate determination of the hole concentration p (see also the Supplemental Material [20]).

Figure 1(f) demonstrates the reversibility of I doping. It shows the differential conductance vs voltage per junction for mesa 2 with $N = 12$ junctions. The initial state (the black curve) is strongly underdoped with a $T_c \simeq 55$ K. After I doping, T_c is increased to 64 K (the blue curve). This strongly affected the intrinsic tunneling spectrum. The sample was remaining in this state for over a week at

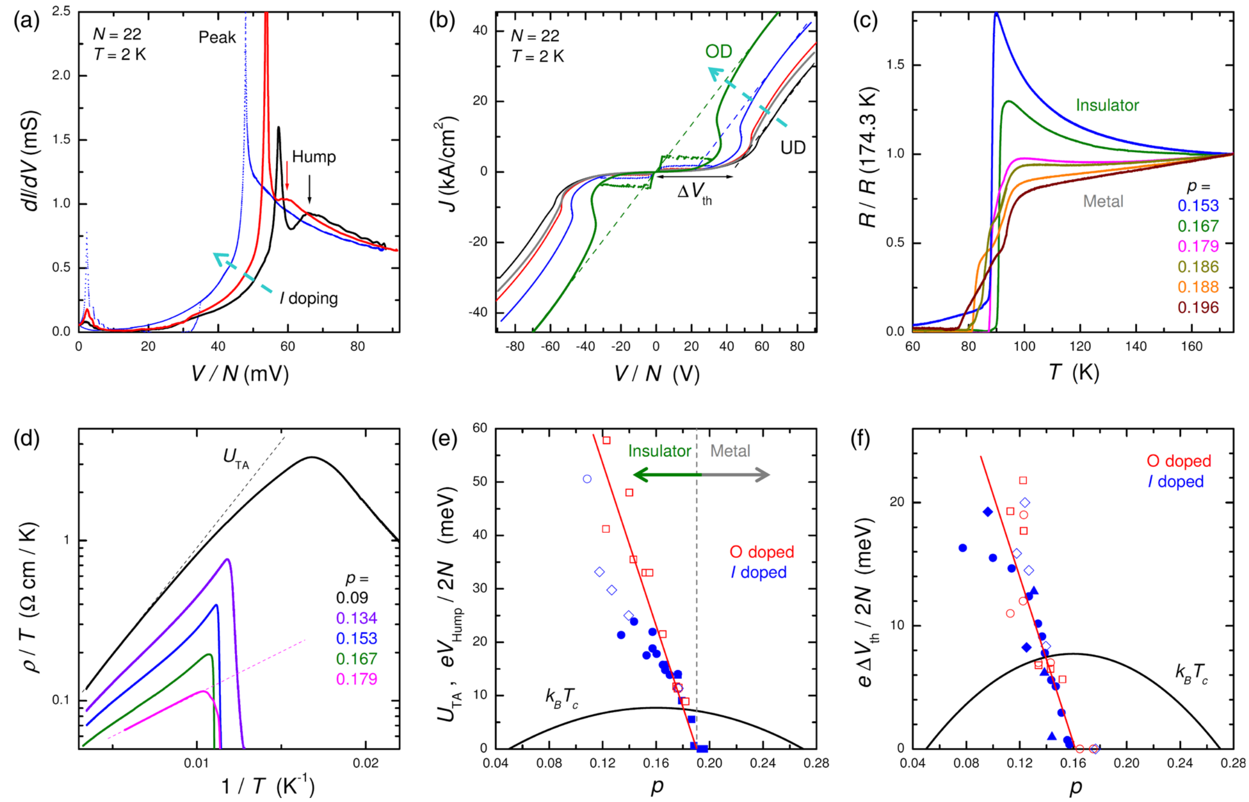

FIG. 2. (a) dI/dV vs V/N at different I-doping states for mesa 1. (b) Normalized current-voltage characteristics of mesa 1 at different doping states from strongly underdoped to slightly overdoped. Dashed lines are extrapolations of the linear sections at high bias. A finite threshold voltage ΔV_{th} appears in the underdoped state. (c) Normalized $R(T)$ curves for I-doped zigzag structures around optimal doping. A metal-to-insulator transition occurs at $p = 0.19$. (d) Thermal-activation plots for zigzag structures. The slope represents the thermal-activation energy U_{TA}. (e) Doping diagram obtained from low-bias characteristics. Open symbols represent the pseudogap energy, $\Delta_{\mathrm{PG}} = eV_{\mathrm{Hump}}/2N$, for I-doped (blue) and O-doped (red) mesa structures. Solid blue symbols represent U_{TA} of I-doped zigzag structures. The critical point at $p = 0.19$ is associated with the onset of the pseudogap and the metal-to-insulator transition in c-axis transport. (f) A doping diagram obtained from high-bias characteristics (threshold voltage). The blue symbols represent I-doped zigzag (solid) and mesa (open) structures. Open red symbols represent ΔV_{th} for O-doped mesas (data from Ref. [8]). Different types of symbols represent different samples.

$T < 100$ K. Subsequently, it was warmed up to room temperature (remaining in a cryostat) and remeasured after a week (the red curve). Apparently, the mesa has relaxed to the initial state. Thus, I doping allows a reversible *in situ* control of the carrier concentration in a broad doping range. We can induce and suppress superconductivity all the way from a nondoped to an overdoped state. This facilitates the investigation of the doping diagram using one and the same sample and removes uncertainties related to sample-to-sample variations, differences in geometrical factors, and cooling conditions.

Figure 2(a) shows dI/dV characteristics of mesa 1 from $p \simeq 0.12$ (the black curve) to $p \simeq 0.14$ (the blue curve). Both a superconducting peak and a pseudogap hump can be seen in the most underdoped state at $p = 0.12$; see also Fig. 1(f). With increasing doping, the peak is rapidly enhanced in amplitude and the hump moves to lower voltage. This indicates that the pseudogap energy $\Delta_{\mathrm{PG}} = eV_{\mathrm{Hump}}/2N$ is decreasing with increased doping. Close to optimal doping, the hump is buried under the peak [8].

Figure 2(b) shows J vs V/N curves for mesa 1. Above the sum-gap kink follows a linear branch [8]. The dashed lines represent extrapolations of those high-bias parts. It can be seen that in the overdoped state, the line passes through zero, but in the underdoped state it extrapolates to some threshold voltage ΔV_{th}, which represents an additional energy required for electron tunneling [8].

Figure 2(c) shows $R(T)$ for zigzag structures close and above optimal doping. It is seen that the upturn in $R(T)$ disappears at $p \gtrsim 0.19$. At larger doping, $R(T)$ exhibits a metallic behavior. Thus, an insulator-to-metal transition in c-axis transport occurs at $p \simeq 0.19$.

The strength of the semiconductor-type $R(T)$ upturn depends on the thermal-activation energy U_{TA} [60]:

$$R/T \propto \exp(U_{\mathrm{TA}}/k_B T). \tag{1}$$

Figure 2(d) shows the corresponding plot $\ln(\rho/T)$ vs $1/T$ for I-doped zigzag structures (ρ is the c-axis resistivity). Slopes (the dashed lines) represent U_{TA}. It is seen that U_{TA} decreases with increased doping.

Figures 2(e) and 2(f) show our main results: doping diagrams of I-doped microstructures together with O-doped mesas from Ref. [8]. The open symbols in Fig. 2(e) represent the pseudogap energy obtained from half of the hump voltage $\Delta_{\mathrm{PG}} = eV_{\mathrm{Hump}}/2N$. The solid blue symbols represent U_{TA} obtained from zero-bias $R(T)$ for I-doped zigzag structures. It can be seen that both Δ_{PG} and U_{TA} consistently point towards a critical point at the overdoped side $p = 0.19$, which corresponds to the onset of the pseudogap. A new perspective, revealed by measurements on zigzag structures without parasitic surface layer contribution, is that there is a simultaneous insulator-to-metal transition in the c-axis transport.

Figure 2(f) represents the high-bias threshold voltage ΔV_{th} obtained by extrapolation of the tunnel resistance branch well above the sum-gap voltage, as marked by the dashed lines in Fig. 2(b) (data for zigzag structures is scaled by factor of 2). Similar to the pseudogap, the threshold voltage also decreases linearly with increased doping and vanishes at optimal doping, $p \simeq 0.16$. Thus, we can distinguish two critical points at $p = 0.19$ and 0.16, suggesting that there is a sequence of quantum phase transitions caused by multiple coexisting orders in cuprates [9,13–15,17,61].

Although critical points at similar doping levels have been reported before [17], to our knowledge two distinct critical points have not been reported with the same technique at one and the same Bi-2212 sample. In our case, the presence of two critical points cannot be explained by specifics of the measurement technique or sample-to-sample variation. The only difference is in the level of bias or energy at which the two critical points are revealed. The critical point at $p = 0.19$ is determined at low energies and the one at $p = 0.16$ at high energies, significantly higher than the pseudogap.

Finally, we want to discuss possible origins of the two critical points. While the one at $p = 0.19$ is caused by the onset of the pseudogap [2–5,8], the interpretation of the other one at $p = 0.16$ is more complex. Generally, high-energy characteristics at $E \gg \Delta$ do not carry information about the gap. Therefore, the threshold voltage usually represents some extra energy required for electron tunneling, such as a capacitive charging energy in small junctions [62], an energy associated with slow dynamic screening of Coulomb interaction in two-dimensional systems [63], inelastic tunneling due to excitation of molecular vibrations or phonons in a tunnel barrier [64], or strong coupling to bosonic modes in the electrodes [65]. In all cases, ΔV_{th} is a consequence of strong correlations with an environment that leads to an enhanced, "dressed" electron energy. Appearance of a dressed energy in underdoped cuprates was reported in Ref. [66].

What is the origin of this dressed energy? Coulomb blocking in this poorly conducting two-dimensional system [63] is one possibility. Alternatively, this could be a signature of any sort of magnetic ordering [67]. Since we are probing only charge degrees of freedom, magnetic order is not directly visible, but it may be seen indirectly via a dressed energy, caused, e.g., by the inelastic excitation of paramagnons. Both the Coulomb blocking energy and the magnetic order should increase upon approaching the antiferromagnetic insulating state, qualitatively consistent with the behavior of the dressed energy. Interestingly, our data indicate that this energy appears at optimal doping, suggesting its intimate connection to high-temperature superconductivity. An anticorrelation between this energy and T_c may imply that the associated "dressing" of electrons is detrimental and may ultimately destroy superconductivity at low doping.

To conclude, we performed *in situ* physical doping of Bi-2212 microstructures by a novel current injection technique. This way we could reversibly tune (induce or suppress) superconductivity and study the doping diagram using one and the same sample. Our results indicated the existence of two distinct critical points: The one at the overdoped side, $p = 0.19$, is associated with the onset of the pseudogap and with a metal-to-insulator transition in the c-axis transport. The second occurs at optimal doping, $p = 0.16$, and is associated with the appearance of a dressed electron energy. Our results, obtained with the same technique at one and the same sample, remove concerns about sample-to-sample variations and technique-specific artifacts of measurements and demonstrate that there is a sequence of quantum phase transitions under the superconducting dome in cuprates.

This work was supported by the Swedish Foundation for International Cooperation in Research and Higher Education Grant No. IG2013-5453, Swedish Research Council Grant No. 621-2014-4314, and Swiss National Science Foundation Sinergia Grant No. CRSII2-154410/1. Technical support from the Core Facility in Nanotechnology at Stockholm University is gratefully acknowledged.

Th. J. and Y. S. contributed equally to this work.

*Vladimir.Krasnov@fysik.su.se

[1] T. Timusk and B. Statt, The pseudogap in high-temperature superconductors: An experimental survey, Rep. Prog. Phys. **62**, 61 (1999).

[2] J. L. Tallon and J. W. Loram, The doping dependence of T*—What is the real high-T_c phase diagram? Physica C (Amsterdam) **349**, 53 (2001).

[3] V. Balédent, D. Haug, Y. Sidis, V. Hinkov, C. T. Lin, and P. Bourges, Evidence for competing magnetic instabilities in underdoped $YBa_2Cu_3O_{6+x}$, Phys. Rev. B **83**, 104504 (2011).

[4] R.-H. He *et al.*, From a single-band metal to a high-temperature superconductor via two thermal phase transitions, Science **331**, 1579 (2011).

[5] I. M. Vishik *et al.*, Phase competition in trisected superconducting dome, Proc. Natl. Acad. Sci. U.S.A. **109**, 18332 (2012).

[6] Th. Jacobs, S. O. Katterwe, H. Motzkau, A. Rydh, A. Maljuk, T. Helm, C. Putzke, E. Kampert, M. V. Kartsovnik, and V. M. Krasnov, Electron-tunneling measurements of low-T_c single-layer $Bi_{2+x}Sr_{2-y}CuO_{6+\delta}$: Evidence for a scaling disparity between superconducting and pseudogap states, Phys. Rev. B **86**, 214506 (2012).

[7] Y. He *et al.*, Fermi surface and pseudogap evolution in a cuprate superconductor, Science **344**, 608 (2014).

[8] V. M. Krasnov, Superconducting condensate residing on small Fermi pockets in underdoped cuprates, Phys. Rev. B **91**, 224508 (2015).

[9] S. Sachdev and B. Keimer, Quantum criticality, Phys. Today **64**, 29 (2011).

[10] K. B. Efetov, H. Meier, and C. Pepin, Pseudogap state near a quantum critical point, Nat. Phys. **9**, 442 (2013).

[11] C. M. Varma, Pseudogap in cuprates in the loop-current ordered state, J. Phys. Condens. Matter **26**, 505701 (2014).

[12] R. Comin, R. Sutarto, E. H. da Silva Neto, L. Chauviere, R. Liang, W. N. Hardy, D. A. Bonn, F. He, G. A. Sawatzky, and A. Damascelli, Broken translational and rotational symmetry via charge stripe order in underdoped $YBa_2Cu_3O_{6+y}$, Science **347**, 1335 (2015).

[13] M. Hücker *et al.*, Competing charge, spin, and superconducting orders in underdoped YBa_2Cu_3Oy, Phys. Rev. B **90**, 054514 (2014).

[14] Y. Wang, D. F. Agterberg, and A. Chubukov, Coexistence of Charge-Density-Wave and Pair-Density-Wave Orders in Underdoped Cuprates, Phys. Rev. Lett. **114**, 197001 (2015).

[15] E. Fradkin, S. A. Kivelson, and J. M. Tranquada, Colloquium: Theory of intertwined orders in high temperature superconductors, Rev. Mod. Phys. **87**, 457 (2015).

[16] N. L. Saini, H. Oyanagi, V. Scagnoli, T. Ito, K. Oka, and A. Bianconi, Different temperature-dependent local displacements in the underdoped and overdoped $La_{2-x}Sr_xCuO_4$ system, Europhys. Lett. **63**, 125 (2003).

[17] S. G. Ovchinnikov, E. I. Shneyder, and M. M. Korshunov, From underdoped to overdoped cuprates: Two quantum phase transitions, J. Phys. Condens. Matter **23**, 045701 (2011).

[18] E. Uykur, K. Tanaka, T. Masui, S. Miyasaka, and S. Tajima, Persistence of the Superconducting Condensate Far above the Critical Temperature of $YBa_2(Cum, Zn)_3O_y$ Revealed by c-Axis Optical Conductivity Measurements for Several Zn Concentrations and Carrier Doping Levels, Phys. Rev. Lett. **112**, 127003 (2014).

[19] A. Dubroka *et al.*, Evidence of a Precursor Superconducting Phase at Temperatures as High as 180 K in $R\,Ba_2\,Cu_3\,\mathbf{O}_{7-\delta}(R = \mathbf{Y}$, Gd, Eu) Superconducting Crystals from Infrared Spectroscopy, Phys. Rev. Lett. **106**, 047006 (2011).

[20] See Supplemental Material at http://link.aps.org/supplemental/10.1103/PhysRevLett.116.067001, which includes Refs. [21–47], for a discussion of doping-phase diagrams of cuprates and additional experimental details.

[21] F. M. Grosche, I. R. Walker, S. R. Julian, N. D. Mathur, D. M. Freye, M. J. Steiner, and G. G. Lonzarich, Superconductivity on the threshold of magnetism in $CePd_2Si_2$ and $CeIn_3$, J. Phys. Condens. Matter **13**, 2845 (2001).

[22] H. v. Löhneysen, A. Rosch, M. Vojta, and P. Wölfle, Fermi-liquid instabilities at magnetic quantum phase transitions, Rev. Mod. Phys. **79**, 1015 (2007).

[23] Q. Si and S. Paschen, Quantum phase transitions in heavy fermion metals and Kondo insulators, Phys. Status Solidi B **250**, 425 (2013).

[24] S. Nandi *et al.*, Anomalous Suppression of the Orthorhombic Lattice Distortion in Superconducting $Ba(Fe_{1-x}Co_x)_2As_2$ Single Crystals, Phys. Rev. Lett. **104**, 057006 (2010).

[25] G. R. Stewart, Superconductivity in iron compounds, Rev. Mod. Phys. **83**, 1589 (2011).

[26] K. Hashimoto *et al.*, A sharp peak of the zero-temperature penetration depth at optimal composition in $BaFe_2(As_{1-x}P_x)_2$, Science **336**, 1554 (2012).

[27] D. van der Marel, H. J. A. Molegraaf, J. Zaanen, Z. Nussinov, F. Carbone, A. Damascelli, H. Eisaki, M. Greven, P. H. Kes, and M. Li, Quantum critical behaviour in a high-T_c superconductor, Nature (London) **425**, 271 (2003).

[28] F. F. Balakirev, J. B. Betts, A. Migliori, I. Tsukada, Y. Ando, and G. S. Boebinger, Quantum Phase Transition in the Magnetic-Field-Induced Normal State of Optimum-Doped High-T_c Cuprate Superconductors at Low Temperatures, Phys. Rev. Lett. **102**, 017004 (2009).

[29] N. Barišić, M. K. Chan, Y. Li, G. Yu, X. Zhao, M. Dressel, A. Smontara, and M. Greven, Universal sheet resistance and revised phase diagram of the cuprate high-temperature superconductors, Proc. Natl. Acad. Sci. U.S.A. **110**, 12235 (2013).

[30] M. Fujita, H. Hiraka, M. Matsuda, M. Matsuura, J. M. Tranquada, S. Wakimoto, G. Xu, and K. Yamada, Progress in neutron scattering studies of spin excitations in high-T_c cuprates, J. Phys. Soc. Jpn. **81**, 011007 (2012).

[31] V. M. Krasnov, Interlayer tunneling spectroscopy of $Bi_2Sr_2CaCu_2O_{8+\delta}$: A look from inside on the doping phase diagram of high-T_c superconductors, Phys. Rev. B **65**, 140504(R) (2002).

[32] B. Vignolle *et al.*, Quantum oscillations and the Fermi surface of high-temperature cuprate superconductors, C.R. Phys. **12**, 446 (2011).

[33] D. LeBoeuf *et al.*, Lifshitz critical point in the cuprate superconductor $YBa_2Cu_3O_y$ from high-field Hall effect measurements, Phys. Rev. B **83**, 054506 (2011).

[34] V. M. Krasnov, A. Yurgens, D. Winkler, P. Delsing, and T. Claeson, Evidence for Coexistence of the Superconducting Gap and the Pseudogap in Bi-2212 from Intrinsic Tunneling Spectroscopy, Phys. Rev. Lett. **84**, 5860 (2000).

[35] V. M. Krasnov, Temperature dependence of the bulk energy gap in underdoped $Bi_2Sr_2CaCu_2O_{8+\delta}$: Evidence for the mean-field superconducting transition, Phys. Rev. B **79**, 214510 (2009).

[36] V. M. Krasnov, H. Motzkau, T. Golod, A. Rydh, S. O. Katterwe, and A. B. Kulakov, Comparative analysis of tunneling magnetoresistance in low-T_c $Nb/Al-AlO_x/Nb$ and high-T_c $Bi_{2-y}Pb_ySr_2CaCu_2O_{8+\delta}$ intrinsic Josephson junction, Phys. Rev. B **84**, 054516 (2011).

[37] S. Hüfner, M. A. Hossain, A. Damascelli, and G. A. Sawatzky, Two gaps make a high-temperature superconductor?, Rep. Prog. Phys. **71**, 062501 (2008).

[38] Ø. Fischer, M. Kugler, I. Maggio-Aprile, Ch. Berthod, and Ch. Renner, Scanning tunneling spectroscopy of high-temperature superconductors, Rev. Mod. Phys. **79**, 353 (2007).

[39] V. J. Emery and S. A. Kivelson, Importance of phase fluctuations in superconductors with small superfluid density, Nature (London) **374**, 434 (1995).

[40] Y. Wang, L. Li, and N. P. Ong, Nernst effect in high-T_c superconductors, Phys. Rev. B **73**, 024510 (2006).

[41] V. M. Krasnov, T. Bauch, and P. Delsing, Probing the intrinsic Josephson coupling potential in $Bi_2Sr_2CaCu_2O_{8+\delta}$ superconductors by thermal activation, Phys. Rev. B **72**, 012512 (2005).

[42] S. O. Katterwe, A. Rydh, H. Motzkau, A. B. Kulakov, and V. M. Krasnov, Superluminal geometrical resonances observed in $Bi_2Sr_2CaCu_2O_{8+x}$ intrinsic Josephson junctions, Phys. Rev. B **82**, 024517 (2010).

[43] V. M. Krasnov, Essence of intrinsic tunneling: Distinguishing intrinsic features from artifacts, Phys. Rev. B **75**, 146501 (2007); Comment on "Counterintuitive consequence of heating in strongly-driven intrinsic junctions of $Bi_2Sr_2CaCu_2O_{8+\delta}$ mesas", Phys. Rev. B **84**, 136501 (2011).

[44] H. B. Wang, S. Guénon, J. Yuan, A. Iishi, S. Arisawa, T. Hatano, T. Yamashita, D. Koelle, and R. Kleiner, Hot Spots and Waves in $Bi_2Sr_2CaCu_2O_8$ Intrinsic Josephson Junction Stacks: A Study by Low Temperature Scanning Laser Microscopy, Phys. Rev. Lett. **102**, 017006 (2009).

[45] V. M. Krasnov, A. Yurgens, D. Winkler, and P. Delsing, Self-heating in small mesa structures, J. Appl. Phys. **89**, 5578 (2001).

[46] V. M. Krasnov, M. Sandberg, and I. Zogaj, In situ Measurement of Self-Heating in Intrinsic Tunneling Spectroscopy, Phys. Rev. Lett. **94**, 077003 (2005).

[47] V. M. Krasnov, Nonlinear Nonequilibrium Quasiparticle Relaxation in Josephson Junctions, Phys. Rev. Lett. **103**, 227002 (2009).

[48] K. Inomata, T. Kawae, K. Nakajima, S.-J. Kim, and T. Yamashita, Junction parameter control of $Bi_2Sr_2CaCu_2O_{8+\delta}$ stacked junctions by annealing , Appl. Phys. Lett. **82**, 769 (2003).

[49] M. Suzuki, T. Watanabe, and A. Matsuda, Interlayer Tunneling Spectroscopy for Slightly Overdoped $Bi_2Sr_2CaCu_2O_{8+\delta}$, Phys. Rev. Lett. **82**, 5361 (1999); M. Suzuki, T. Hamatani, K. Anagawa, and T. Watanabe, Evolution of interlayer tunneling spectra and superfluid density with doping in $Bi_2Sr_2CaCu_2O_{8+\delta}$, Phys. Rev. B **85**, 214529 (2012).

[50] H. Kambara, I. Kakeya, and M. Suzuki, Increase of superfluid density with growth of quasiparticle density of states probed by intrinsic tunneling spectroscopy in $Bi_{1.9}Pb_{0.1}Sr_2CaCu_2O_{8+\delta}$, Phys. Rev. B **87**, 214521 (2013).

[51] Y. Koval, X. Jin, C. Bergmann, Y. Simsek, L. Özyüzer, P. Müller, H. Wang, G. Behr, and B. Büchner, Tuning superconductivity by carrier injection, Appl. Phys. Lett. **96**, 082507 (2010).

[52] H. Motzkau, Th. Jacobs, S.-O. Katterwe, A. Rydh, and V. M. Krasnov, Persistent electrical doping of $Bi_2Sr_2CaCu_2O_{8+x}$ mesa structures, Phys. Rev. B **85**, 144519 (2012).

[53] Y. Simsek, Y. Koval, K. Gieb, and P. Müller, Superconductivity induced by carrier injection into non-superconducting $Bi_2Sr_2CaCu_2O_{8+\delta}$Supercond. Sci. Technol. **27**, 095011 (2014).

[54] C. H. Ahn *et al.*, Electrostatic modification of novel materials, Rev. Mod. Phys. **78**, 1185 (2006).

[55] A. T. Bollinger, G. Dubuis, J. Yoon, D. Pavuna, J. Misewich, and I. Boźović, Superconductorinsulator transition in $La_{2-x}Sr_xCuO_4$ at the pair quantum resistance, Nature (London) **472**, 458 (2011).

[56] K. Ueno, S. Nakamura, H. Shimotani, H. T. Yuan, N. Kimura, T. Nojima, H. Aoki, Y. Iwasa, and M. Kawasaki, Discovery of superconductivity in $KTaO_3$ by electrostatic carrier doping, Nat. Nanotechnol. **6**, 408 (2011).

[57] X. Leng, J. Garcia-Barriocanal, B. Yang, Y. Lee, J. Kinney, and A. M. Goldman, Indications of an Electronic Phase Transition in Two-Dimensional Superconducting $YBa_2Cu_3O_{7-x}$ Thin Films Induced by Electrostatic Doping, Phys. Rev. Lett. **108**, 067004 (2012).

[58] V. I. Kudinov, I. L. Chaplygin, A. I. Kirilyuk, N. M. Kreines, R. Laiho, E. Lähderanta, and C. Ayache, Persistent photoconductivity in $YBa_2Cu_3O_{6+x}$ films as a method of photodoping toward metallic and superconducting phases, Phys. Rev. B **47**, 9017 (1993).

[59] D. Fausti, R. I. Tobey, N. Dean, S. Kaiser, A. Dienst, M. C. Hoffmann, S. Pyon, T. Takayama, H. Takagi, and A. Cavalleri, Light-induced superconductivity in a stripe-ordered cuprate, Science **331**, 189 (2011).

[60] S. O. Katterwe, A. Rydh, and V. M. Krasnov, Doping-Induced Change in the Interlayer Transport Mechanism of $Bi_2Sr_2CaCu_2O_{8+\delta}$ near the Superconducting Transition Temperature, Phys. Rev. Lett. **101**, 087003 (2008).

[61] B. J. Ramshaw *et al.*, Quasiparticle mass enhancement approaching optimal doping in a high-T_c superconductor, Science **348**, 317 (2015).

[62] D. V. Averin, A. N. Korotkov, and K. K. Likharev, Theory of single-electron charging of quantum wells and dots, Phys. Rev. B **44**, 6199 (1991).

[63] F. G. Pikus and A. L. Efros, Coulomb gap in a two-dimensional electron gas with a close metallic electrode, Phys. Rev. B **51**, 16871 (1995).

[64] J. Lambe and R. C. Jaklevic, Molecular vibration spectra by inelastic electron tunneling, Phys. Rev. **165**, 821 (1968).

[65] J. Lee *et al.*, Interplay of electronlattice interactions and superconductivity in $Bi_2Sr_2CaCu_2O_{8+\delta}$, Nature (London) **442**, 546 (2006).

[66] F. Novelli *et al.*, Witnessing the formation and relaxation of dressed quasi-particles in a strongly correlated electron system, Nat. Commun. **5**, 5112 (2014).

[67] Generally, it can be due to strong coupling to any bosonic mode, including phonons. However, it is not obvious why the phononic mode would disappear above optimal doping.